6/1 7/94

ELECTRON EXCITATION CROSS SECTIONS FOR THE $2s^2 2p^3\ ^4S^0 \rightarrow 2s^2 2p^3\ ^2D^0$ (FORBIDDEN) AND $^4S^0 \rightarrow 2s2p^4 4P$ (RESONANCE) TRANSITIONS IN *OII*

M. Zuo[†], Steven J. Smith, A. Chutjian, I. D. Williams*

Jet Propulsion Laboratory, California Institute of Technology
Pasadena, California 91109

S. S. Tayal

Department of Physics and Astronomy
Clark Atlanta University, Atlanta, Georgia 30314

Brendan M. McLaughlin

Institute for Theoretical Atomic and Molecular Physics
Harvard-Smithsonian Center for Astrophysics
Cambridge, Massachusetts 02138

ABSTRACT

Experimental and theoretical excitation cross sections are reported for the first forbidden transition $^4S^0 \rightarrow 2s^2 2p^3\ ^2D^o$ ($\lambda\lambda$ 3726, 3729 Å) and the first allowed (resonance) transition $^4S^0 \rightarrow 2s2p^4\ ^4P$ (λ 834 Å) in OII. Use is made of electron-energy loss and merged-beams methods. The electron energy range covered is 3.33 eV (threshold) to 15 eV for the S → D transition, and 14.9 eV (threshold) to 40 eV for the S → P transition. Care was taken to assess and minimize the metastable fraction of the OII beam. An electron mirror was designed and tested to reflect inelastically back-scattered electrons into the forward direction to account for the full range of polar scattering angles. Comparisons are made between present experiments and 11-state *R*-Matrix calculations. Calculations are also presented for the $^4S^0 \rightarrow 2s^2 2p^3\ ^2P^o$ (λ 2470 Å) transition.

[†] Present address: Physics Dept., University of Colorado, Boulder, CO 80309

* Permanent address: Dept. Pure and Applied Physics, The Queen's University Belfast BT7 1 NN, United Kingdom

PACS Classification No.: 34.80 Kw

1. INTRODUCTION

The electron (collisional) excitation of singly- and multiply-charged positive ions using energy-loss methods is a relatively new and unexplored area of research, The phenomenon occurs in a wide range of plasmas, extending from X-ray lasers (Nilsen 1993) to tokamaks (Bitter *et a/. 1993).* Collisional excitation of transitions in 0// have most recently been observed in the lo-Jupiter torus by the Goddard High-Resolution Spectrograph aboard the Hubble Space Telescope (HST) (McGrath *et a/.* 1993) and by the Hopkins Ultraviolet Telescope (Moos *et a/. 1991).* Emissions from collisionally-excited 0// are also prevalent in Seyfert Galaxy spectra, as seen for example by the Faint Object Spectrograph on the HST (Caganoff *et a/. 1991;* Kriss *et a/. 1991).*

Accurate collision strengths are required for understanding energy balance and rates of radiative decay in the various plasmas (Smith *et a/.* 1993a). In equations of plasma statistical equilibrium the collisional excitation rate $C(g \rightarrow i)$ plays a central role in calculating level populations and line-emitted power (Gabriel & Jordan 1972; Mason & Monsignori-Fossi 1994). For a simple high-density, two-level system, the population N_i of level i can be expressed as

$$N_i = \frac{N_e N_g C(g \rightarrow i)}{A(i \rightarrow g)} \qquad (1)$$

where N_e is the electron density, N_g the emitter ground-level density, $A(i \rightarrow g)$ the spontaneous radiative decay rate i to g, and $C(g \rightarrow i)$ the electron collisional rate coefficient for the transition $9 \rightarrow i$. The collisional rate in turn can be expressed in terms of an effective collision strength Υ (g, i) as (McLaughlin & Bell 1993a)

$$\Upsilon(g, i) = \int_0^\infty \Omega_{gi}(X) \exp\left[-\frac{\epsilon_g}{kT_e}\right] d\left(\frac{\epsilon_g}{kT_e}\right) \quad (2)$$

where T_e is the peak temperature of the Maxwellian electron velocity distribution, X is the center-of-mass (CM) energy in threshold units, and ϵ_g is the incident electron energy for *OII* in its ground (initial) state g. The cross section u(X) (quantity reported here) is related to the collision strength $\Omega_{gi}(X)$ by the standard expression

$$\sigma_{gi}(X) = \frac{\Omega_{gi}(X)}{\omega_g}[X \cdot E_{gi}]^{-1} \quad (3)$$

where E_{gi} is the transition energy in Ry, $\sigma(X)$ is in atomic units (πa_o^2) and $\omega_g = (2S_g + 1)(2L_g + 1)$ for *LS* coupling.

There are no experimental measurements of collisional excitation cross sections in *OII*. On the other hand, there are several theoretical calculations for excitation from the ground $^4S^o$ to the first $^2D^o$ and 4_p states. These were carried out in a 3-state close-coupling approximation (Henry *et al.* 1969), a 2-state NIEM approach (Ho & Henry 1983), and in several R-matrix levels of approximation (McLaughlin *et al, 1987;* McLaughlin & Bell 1993a, 1993b). Presented herein are the first experimental results and new theoretical (11 -state close coupling) calculations for the transitions $^4S^o \rightarrow 2s^2 2p^3\, ^2D^o$ (forbidden) and $^4S^o \rightarrow 2s2p^4\, 4_p$ (resonance); and theoretical calculations for the $^4S^o \rightarrow 2s^2 2p^3\, 2P^o$ (forbidden) transition. A partial energy-level diagram of *OII* is given in Figure 1. The experiments were carried out using electron energy-loss, merged-beams methods (Smith *et al. 1991,* 1993b). Experimental details are given in Sec. *II*, including (a) verification of the metastable content of the target *OII* beam (Sec. *II. A),* (b) using a new electron mirror, experimental measurement of the entire angular range of inelastically-scattered electrons, rather than

partial reliance on theory to obtain integra cross sections (Sec. *//. B),* and (c) other refinements in the measurements, including analysis of evaluation of dead-time corrections using separate bins for the four phases of electron-ion beams modulation (Sec. *//.* C). The theoretical R-matrix methods are discussed in Sec. ///, and experimental cross sections with comparison to theory reported in *Sec. /V.*

II. EXPERIMEN`AL METHODS

The experimental arrangement is shown schematically in Figure 2. The apparatus and the merged-beams, electron energy loss technique have been described in detail in a previous publication (Smith et *a/.* 1993 b). Given here is an overview of basic techniques before describing in more detail recent enhancements, and methods used to overcome problems specific to the 0// target.

A beam of 0// ions extracted from a Colutron ion source was momentum-analyzed by a 60° bending magnet and focused through differentially-pumped regions into the interaction chamber, which was maintained at a base pressure of 10^{-7} Pa. Low energy electrons, confined by a uniform, axial solenoidal magnetic field B = 0,0055 T were merged with the 0// beam through trochoidal deflection in the merging plates MP. Spatial profiles of the beams and overlap form factors were monitored by rotating vanes at four points along the 20 cm merged-path. Inelastically scattered electrons were separated from the primary electron beam by trochoidal deflection in the analyzing plates AP, and subsequently collected by a position sensitive detector (PSD). The PSD was used in conjunction with grids to discriminate between high axial-energy and low axial-energy electrons (Smith *et a/.* 1993b). The primary electron beam was further deflected in plates

DP, out of the plane containing MP and AP, and collected in a deep Faraday cup, An electron mirror Ml was used to reflect inelastically back-scattered electrons to the forward PSD. The ion beam passed straight through plates AP and was focused into a second deep Faraday cup. Baffling was employed to reduce background contributions from any slow primary or secondary electrons escaping from the Faraday cups,

"There is in general some degree of spatial overlap between elastically and inelastically scattered electrons on the PSD. To first order only those particles with forward (axial) velocity components equal to that of the inelastic signal may be transmitted through the analyzer and strike the detector, However, due to the larger Larmor radii of the elastically scattered electrons, the range of transmitted velocities through the trochoidal analyzer is increased as off-axis particles are accelerated or retarded to within the range of pass-velocities of the analyzer, On exiting the analyzer plates these particles regain their original forward velocity component, and may be discriminated against by applying a suitable bias on parallel grids mounted in front of the PSD. Techniques used to subtract the remaining underlying elastic contribution from the inelastic signal have been previously described in detail (Smith *et a/.* 1993b).

A double-beams modulation technique was used to enhance the signal-to-noise ratio. Typically, signal from the PSD was routed to a histogramming memory unit, and the channel associated with the electron's (x, *y)* position incremented or decremented by unity, depending on the modulation phase. In the present study a different acquisition technique was also used, Four separate histogramming memory units were utilized, with each unit collecting signal from a distinct phase. This allowed one to apply the dead-time correction appropriate to the count rate in that phase, as well as simplifying the correction process (see also Sec. *//.* C). The four different modulation phases are A: electron beam off,

ion beam off; *B*: electron beam on, ion beam on; C: electron beam on, ion beam off; *D*: electron beam off, ion beam on.

Cross sections were obtained from the relationship,

$$u(E) = \frac{Re^2\mathcal{F}}{\epsilon I_i I_e L} \left| \frac{v_e v_i}{v_e - v_i} \right| \qquad (4)$$

where R is the total signal rate (s-l), e the electron charge, /e and /j the electron and ion currents (A) respectively, L the merged path length (cm), ϵ the detector efficiency of the PSD, $\mathcal{F}$ the overlap factor between the electron and ion beams (cm^{-2}), and $\sigma(E)$ the excitation cross section (cm^2).

A. Determination of the Metastable Fraction in the 0// Beam

Ion beams produced in accelerator sources often contain a significant fraction *f* of metastable states. The population will depend on the ion quantum levels involved (*via* their lifetimes), ion transit time from source to scattering region, and the operating conditions of the source (anode current, anode voltage, *rf* or microwave power, gas pressure, etc.). If the excited-state population is *not* known, then in any state-to-state cross section measurement only some fraction *(l-f)* of the ion beam contributes to the scattered signal, while the entire beam is counted in measurement of the ion current. And hence the measured cross section is smaller by the factor *1/(1-f)* than its true value, The metastable levels in 0// which can be significantly populated (Figure 1) are $^2D^o$ and 2P" (Lee *et al.* 1991).

10 measure the metastable population a method was used (Turner *et al. 1968;* Gilbody 1978) wherein an ion beam is attenuated in a gas-filled section of the ion beam

line, and the transmitted ion beam current is measured as a function of gas pressure. Since different electronic states of the ion usually have different charge-exchange cross sections, one will observe breaks in the slope of transmitted current *vs* pressure corresponding to attenuation by different excited states. Extrapolation of the high-pressure slope (corresponding to charge-exchange by the ground state) to zero gas pressure will yield the metastable fraction of the beam.

'The section of ion beam line in the ion-source area (region of *L1* in Figure 2) was filled with the attenuating gas, in this case argon. The transmitted ion current was measured on the central element of lens system L2 as a function of *Ar* pressure. Results are shown in Figure 3. Attenuation of a 4 keV 0// beam in argon was measured as a function of relative argon pressure under two ion-source conditions: one in which the source was run with a high filament current and high anode voltage (open circles O), and one in which the current and voltage were kept at their lowest levels consistent with stable ion production (crosses +). A clear discontinuity in slope is seen for the former case. When the high-pressure slope is extrapolated to zero *Ar* pressure one obtains a metastable fraction $f = 0.20$. No detectable break in slope was seen for the low current-voltage case, indicating a metastable fraction of $f \leq 2\%$. An uncertainty of *2%* in the final cross section was assigned due to possible metastable contamination (see Table 1).

B. The Electron Mirror

In order to reflect electrons that are inelastically-scattered through laboratory angles in the range $90° < \vartheta \leq 180°$ a three-element lens system was designed with the center potential adjusted to act as a mirror to the back-scattered electrons (Spangenberg 1948).

The operation of the mirror, as immersed in a uniform magnetic field, is illustrated in the schematic of the lens system in Figure 4. Shown are the associated contours of the electric field, and electron trajectories for five laboratory polar scattering angles (ϑ = 92, 114, 136, 158, and 180°) at incident electron energies E_e = 0.50, 2.0 and 15 eV. The laboratory azimuthal scattering angle φ was held fixed at φ = 0°, so that the pattern shown in Figure 4 represents one trajectory of a fuller pattern sampled for φ {0,3600}. All such trajectories cleared the apertures of the mirror at the highest design energy (15 eV) studied. [Note: the font ϑ,φ refers to LAB angles, while the font θ,ϕ refers to CM angles.]

As can be seen from Figure 4 electrons with high axial kinetic energy (scattered through angles near 180°) penetrate the inner portion of the lens in which the field lines are concave, while those with low axial and high radial energy (scattered through angles near 90°) are reflected before reaching the center, at the convex-shaped field lines. The indicated voltages on the mirror are the lowest voltages (in absolute magnitude) at which the mirror will reflect; *i.e.*, the ϑ = 180° ray stops to the left, just short of lens center (not quite over the central hump of the saddle potential).

The electron lens system was fabricated of CP titanium. For testing purposes, it was inserted immediately to the left of the analyzing plate AP (Figure 2). Electrons from the gun were launched into the mirror, back-reflected, and the current measured on a Faraday cup placed at the position of lens system *L4*. An additional trochoidal deflector (not shown) was placed in front of this Faraday cup to assist in tuning the back-reflected beam into the Faraday cup over a range of incident electron energies. The transmitted electron beam was detected in the "Electron Cup" (Figure 2).

A series of measurements were carried out in which both the transmitted and back-reflected electron currents were measured as a function of lens potentials, at electron

energies in the range 0.20 eV $\leq E_o \leq$ 20 eV. Agreement of the applied lens potentials with the SIMION-calculated (Dahl & Delmore 1988) potentials was found. The reflectivity (reflected current to the back cup divided by transmitted current to the forward cup) was found to be 99 ± *2?40* in this energy range. The cross sections reported herein were measured with the SIMION-calculated potentials, as verified by the experimental measurements.

C. Dead-Time Corrections

Precise dead-time corrections must be made to the raw data from the histogramming memory, since the subtracted rate is small by comparison to rates present in the individual modulation phases *B* and *D*. The method used to apply a single dead-time correction to the final subtracted rate has been described in detail in Smith etaL(1993b).

The acquisition system has recently been modified by routing signals from phases *A, B, C,* and *D* into four separate histogramming memory units. This permits the application of dead-time corrections to each individual measured rate [A], [b], [C], [$\dot{D}$] to give the true (t) individual rates [Al,, [B],, [Cl,, [b], . The true count rate is then given by $R = [\dot{A}]_t + [\dot{B}]_t - [\dot{C}]_t - [\dot{D}]_t$. This considerably simplifies the correction procedure.

Counts from the PSD above a set discrimination level are digitized by computing electronics to give (x, y) addresses, then stored in the histogramming memory. This 'strobe' channel of the computing electronics has an associated dead-time of 3.0 ± 0.1 μs. The total rate at which electrons strike the PSD is monitored by a PC-based counter. This 'rate' channel has an associated dead-time of 0.45 ± 0,05 μs. The 'rate' counter is gated to measure individual rates for each of the four phases, which may then be used to correct

the signals in the 'strobe' channel. Both channels behave as paralyzable elements, and hence the relevant formula as discussed by Lampton & Bixler (1 985) was used to compute the respective correction factors.

A number of data points in 0// were obtained with the enhanced data acquisition system, together with several points using *MgII* and *ZnII* targets for comparison with previous data (Smith *et a/. 1991,* 1993b). At all energies agreement between the old and new methods for the three ions was within the limits of uncertainty. The new method is now the preferred way of taking data, and will be the method used in future studies.

III. THEORETICAL CONSIDERATIONS

Cross sections have been calculated for electron-impact excitation from the I@2s~2p^{3}4S" ground state configuration of Onto the $1s^2 2s^2 2p^3$ *D", $1s^2 2s^2 2p^3$ $^2P^o$, and the $1s^2 2s 2p^4$ 4_p *levels.* The cross sections were obtained from collision strengths calculated using the *ab initio* R-matrix approximation with multiconfiguration-interaction target wave functions in the *LS* coupling scheme.

In the present work, the lowest eleven states were retained in the multi-configuration expansion of the *OII* target wave functions namely $1s^2 2s^2 2p^3$ $^4S^o, ^2D^o, ^2P^o$; $1s^2 2s 2p^4$ 4P, ^2D, 2P, ^2S; and $1s^2 2s^2 2p^2 3s$ $^4P, ^2D$, 2P, ^2S. The target wave functions were those obtained by Bell *et a/. (1* 989) which have provided reliable results for photoionization of neutral oxygen (Bell *et* a/. 1989, 1990), and for electron impact excitation of 0// (McLaughlin & Bell 1993a, 1993c, 1994a, 1994 b).

The initial states of the e-O// collision complex are represented as superpositions of bound eight-electron states and states descriptive of an 0// ion plus a free electron. The

corresponding R-matrix basis functions are of the form

$$\Psi_k = A \sum_{i,j} c_{ijk}\, \Phi_i\,(x_1, x_2, \ldots \hat{r}_8\sigma_8)\, u_{ij}(r_8) + \\ + \sum_j d_{jk}\, \phi_j(x_1, x_2, \ldots, x_8)\,. \qquad (5)$$

Here A denotes the antisymmetrization operator and xi stands for the space and spin coordinates $r_i\sigma_i$ of the i^{th} electron. The channel functions Φ_i appearing here are eigenstates of L, S and π (parity), formed by coupling a wavefunction of the O_{II} ion to that for the orientational and spin coordinates of the ejected electron. The u_{ij} are continuum functions describing the radial motion of the scattered electron. The radial part of each orbital is expressed in analytical form as a sum of Slater-type orbitals. The 1s, 2s, and 2p radial functions are those of the $2p^3\,^4S^0$ ground state given by Clementi and Roetti (1 974), while the 3s, 3p, and 3d orbitals are taken from Bell *et al.* (1 989). The parameters of the wavefunctions together with the configurations used to describe the O_{II} states and the excitation energies are listed in Bell *et al.* (1 989). The ϕ_j are eight-electron bound-state wavefunctions which account for polarization and short-range correlation effects including intermediate resonance states of neutral atomic oxygen. The coefficients c_{ijk} and d_{jk} were obtained by diagonalizing the Hamiltonian in the inner region $r \leq a$ bounded by the R-matrix boundary a.

Each of the R-matrix basis functions Ψ_k includes eleven O_{II} states and thirty Lagrange-orthogonalized continuum orbitals. An R-matrix radius of $a = 12.4\ a_o$ was required to accommodate the diffuse pseudo-orbitals. For each $LS\pi$ symmetry the R matrix was calculated at this boundary and matched to solutions in the outer region to obtain the appropriate K matrix, from which the T and S matrices and the appropriate collision

strength $\Omega_{ij}(X)$ were then obtained. The theoretical threshold energies of the 0// ion were shifted to the experimental values before the diagonalization o' the $(N+1)$ electron Hamiltonian was carried out in the inner region. This ensured that resonances and thresholds were correctly positioned,

The F?-matrix/Opacity computer codes (Barrington *et al. 1978,* 1987) were used to perform all electron collision-strength calculations. The relevant theory has been outlined in Burke & Robb (1 975), Seaton (1 987) and Burke (1 993). Calculation of the collision strengths Ω_{ij} {X) was carried out at a fine energy mesh of 10-4 Ry in the region between thresholds so that the complex resonance structure could be fully resolved for the transition of interest. At each electron impact energy, collision strengths were obtained by calculating contributions for each total $LS\pi$ symmetry, For total angular momentum $L \leq 70$ the full-exchange R-matrix method was used. Contributions to the collision strength for total angular momentum $77 < L \leq 60$ were then obtained using the non-exchange approach of Burke *et al.* (1 992). Higher-L contributions to the collision strength were estimated using criteria outlined by Burgess & Seaton (1 960) and by Burgess eta*l.* (1 970). The pseudo-resonances that appear in the total collision strengths above all thresholds were then averaged over. Further details of the 0// collision calculations may be found in McLaughlin & Bell (1993a).

From the S and T matrices one then has the relevant scattering information to calculate the DCS $d\sigma/d\Omega$ as a function of scattering angle θ at a specific energy. This is an important quantity since integration of $d\sigma/d\Omega$ over appropriate angular ranges may be compared with scattering results using the electron mirror, and used to account for overlapping transitions.

IV. RESULTS AND DISCUSSION

In the reduction of the experimental data, care was taken to account for overlap of the true $^4S^0 \rightarrow {}^2D^0$ and $^4S^0 \rightarrow 4_p$ signals by electrons elastically scattered through large angles, and by inelastic contributions from transitions to adjacent states. The method used to subtract the underlying elastic background has been dealt with in detail in Smith *et al.* (1993b). It relies on the fact that the elastic contribution is broadly distributed over the entire PSD whereas the inelastic signal is typically peaked in a well defined area. The maximum uncertainty induced by the subtraction procedure is 7% *(see* Table 1).

To calculate the contribution from inelastically-scattered electrons due to transitions to adjacent states, a different technique was used. Electron-trajectory calculations with the SIMION code were carried out to estimate the fraction of electrons, scattered by competing processes, striking the PSD. Only a limited range of ϑ, φ scattering angles contribute, depending on parameters such as analyzer plate voltages, and LAB-to-CM angle transformation. At each ϑ the product of the fraction striking the PSD, and the DCS at that ϑ is calculated. The products are summed over all ϑ giving the total adjacent-state contribution.

Present theoretical DCS were used to compute the $^4S^0 \rightarrow {}^2P^o$ contribution to the $^4S^0 \rightarrow {}^2D^o$ signal, and the $^4S^0 \rightarrow {}^2D^0$ contribution to the $^4S^0 \rightarrow 4_p$ signal. For the $^2D^0$ cross sections, the subtracted $^2P^o$ component averaged about 12°A of the total. In the 4_p case, the $^2D^o$ contributions averaged about 10%, while the 2P" contribution to the 4_p signal was negligible. This was partly due to the smaller 2P" cross section, and partly due to the analyzer's enhanced resolution for the states well-separated in energy. In general, the extent of overlapping will depend on the relative magnitudes of the *u(E)* and their DCS.

The uncertainty introduced to the measured cross sections due to this procedure is estimated to be *2%* (see Table 1),

Since one has only a single PSD in the forward direction, a correction ratio R has to be applied to account for inelastically-backscattered electrons having $\vartheta > \pi/2$. It is defined by

$$\mathbb{R} = \frac{2\pi \int_{0}^{\pi} (d\sigma/d\Omega) \sin\theta \, d\theta}{2\pi \int_{0}^{\theta_{CM}^{max}} (d\sigma/d\Omega) \sin\theta \, d\theta} \qquad (6)$$

where $(d\sigma/d\Omega)$ *is* the DCS for the relevant transition, and where θ_{CM}^{max} is the maximum CM angle corresponding to scattering at ϑ = 90° collection in the LAB frame,

In earlier work the ratio $\mathbb{R}$ was calculated from theory (Smith *et a/. 1993b).* In the present work R was still for the most part calculated from theoretical DCS. R was also determined experimentally by taking the ratio of a measurement made with the mirror voltage "on", to a measurement made with the mirror voltage "off". These measurements were carried out at several energies, for both the $^2D^o$ and 4_p transitions, giving good agreement with R as calculated from the DCS. Values of R are given in Tables 2 and 3 for the $^2D^o$ and 4_p transitions, respectively, The uncertainty in this correction is estimated to be *5%* (Table 1).

Note that near each excitation threshold no correction for overlapping contributions or incomplete collection is necessary. Away from threshold, use of the electron mirror makes the latter correction unnecessary.

A. Experimental-Theoretical Results for the $^4S^0 \rightarrow {}^2D^0$ (Forbidden) Excitation

Experimental and theoretical results for the $^4S^0 \rightarrow {}^2D^0$ excitation are given in Table 2 and presented in Figures 5 and 7. Displayed in Figure 5 is the theoretical DCS, calculated as described by Smith (1 971), in the range $\theta\{0,\pi\}$ at several CM energies between 4.0 and 12.0 eV. Near threshold the DCS is found to be almost isotropic, the cross section being dominated by s-wave scattering. At 3-4 times threshold the DCS becomes more strongly backward-peaked. This was confirmed experimentally at 10.0 eV, where the ratio R was measured using the electron mirror, giving good agreement with theory. Clearly electron exchange effects leading to high-angle scattering are important at the 9 and 12 eV energies.

Integral cross sections for the $^4S^0 \rightarrow$ *D" excitation are presented in Figure 7. For comparison with experiment the theoretical cross sections have been convoluted with an experimental Gaussian energy beam distribution of 250 meV full width at half maximum (FWHM). The experimental cross sections are seen to be strongly peaked at threshold, with a value of about 1.25 x 10^{-16} cm^2, and decrease rapidly as a function of energy out to 3 times threshold. They are in good agreement with the present 11 -state R-matrix calculations, and also with the 2-state close-coupling calculations of Henry *et al. (1* 969). The 1 l-state theory is found to lie approximately 10% below the earlier 2-state theory,

The uncertainty in the experimental data is made up of individual uncertainties listed in Table 1. Individual uncertainties are listed at the 1σ confidence level, and the total quadrature uncertainty is cited at the 1.7σ (90%) confidence level (CL) of random error. Because of the former method of dead-time correction, this individual uncertainty is added linearly to the quadrature combination of the remaining uncertainties (Smith *et al.* 1993b).

The total 1.70 uncertainty in the experimental cross sections is $^{+21}_{-19}$%. This experimental uncertainty allows one to clearly place upper and lower bounds to theory, but does not allow one to resolve the 10% difference between the calculations.

B. Experimental-Theoretical Results for the $^4S^0 \rightarrow 4_P$ (Resonance) Excitation

Experimental and theoretical results for the $^4S^0 \rightarrow 4_P$ excitation are listed in Table 3 and presented in Figures 6 and 8. Shown in Figure 6 are calculated DCS for excitation of the 4_P state at collision energies between 16 and 25 eV. The DCS are seen to be peaked in the forward direction for all energies studied, as one would expect for resonance excitation in singly-charged ions. This is in marked contrast to the observation for the *D" transition. Experimental measurements of R at 16.5 and 25.0 eV confirm the dominance of low-angle scattering for this transition. The oscillations in the DCS observed at larger scattering angles are indicative of interference between low partial-wave components.

Integral cross sections, measured and calculated, are presented in Figure 8 for the energy range from threshold to 40.0 eV. As for the $^2D^0$ transition, the experimental data are in good agreement with the present theory, and confirm the precision of the theoretical calculations to within 20%. The 2-state close-coupling calculations of Ho & Henry (1983) are also found to lie within present experimental uncertainties. The 4_P cross section is found to be slowly varying over the energy range studied, displaying a broad peak centered at about 1.5 times threshold. The peak value of about 0.6 x 10^{-18} cm^2 is significantly lower than the threshold peak value for the forbidden *D" transition.

C. Theoretical Results for the $^4S^o \rightarrow {}^2P^o$ (Forbidden) Excitation

Theoretical calculations for the 2P" transition are presented in Table 4, for collision energies in the range 5.5 -25.0 eV. The cross section behaves in a similar way to that for the $^2D^{c)}$ transition, peaking sharply at threshold and falling rapidly as a function of collision energy. The threshold peak value is however almost an order of magnitude less than for the $^2D^o$ transition. For this reason it has been difficult to obtain quantitative experimental data for the 2P" transition. The weak nature of the $^4S^0 \rightarrow$ 2P" energy-loss feature observed near threshold (Smith *et a/. 1993a)* is consistent with the small value of cross section predicted by the 11-state theory.

ACKNOWLEDGEMENTS

Part of the calculations were performed at the Minnesota Supercomputer Center on the CrayYMP-C90/8P/512MW, B. McL. thanks the Minnesota Supercomputer Institute for grants of computing time, and a visiting research scholarship during the course of this work. The Institute for Theoretical Atomic and Molecular Physics at the Harvard Smithsonian Center for Astrophysics is supported by a grant from the National Science Foundation. SST thanks the US Department of Energy, Basic Energy Sciences, and the National Science Foundation. Generous supercomputertime on the NERSC supercomputers provided by the US DoE is appreciated. MZ and IDW thank the NASA-National Research Council for support at JPL. Experimental measurements were carried out at the Jet Propulsion Laboratory, California Institute of Technology, and supported by the National Aeronautics and Space Administration.

REFERENCES

Bell K. L., Barrington K. A., Burke P.G., Hibbert A., & Kingston, A. E. 1990, *J. Phys. B, 23, 2259*

Bell K. L., Burke P. G., Hibbert A., & Kingston, A. E. 1989, *J. Phys. B, 22, 3197*

Berrington K. A., Burke P. G., Butler K., Seaton M. J., Storey P, Taylor K. T., & Yu Yan 1987, *J. Phys. B, 20, 6379*

Barrington K. A., Burke P. G., LeDourneuf M., Robb W. D., Taylor K. T., & and Vo Ky Lan 1978, *Comput. Phys. Commun., 14, 367*

Bitter M., Hsuan H., Hill, K. W. & Zarnstorff M. 1993, *Physics Scripts, T47, 87*

Burgess A., Hummer D. G., & Tully J. A. 1970, *Phil. Trans. Roy. Sot. London, Ser. A, 226, 225*

Burgess A., & Seaton M. J. 1960, *Mon. Not. Royal Astron. Sot., 120, 121*

Burke P. G. 1993, in *A/P Conference Proceeding 295,* ed. T. Andersen, B. Fastrup, F. Folkmann, H. Knudsen, and N. Andersen (New York: Am, Inst. Phys.), p. 26.

Burke P.G., & Robb W. D. 1975, *Adv. At. Mel. Phys., 77, 143*

Burke V. M., Burke P. G., & Scott N. S. 1992, *Comput. Phys. Commun., 69, 76*

Caganoff S., Antonucci R. R. J., Ford H. C., Kriss G. A., Hartig G., Armus L., Evan I. N., Rosenblatt E., Bohlin R. C., & Kinney A. L. 1991, *Astrophys. J., 377, L9*

Clementi E., & Roetti C. *1974, At. Data Nucl. Data Tables, 14, 177*

Dahl D, A. & Delmore J, E. 1988, Idaho National Engineering Laboratory Report No. EGG-CS-7233 Rev. 2 (unpublished)

Gabriel A. H., & Jordan C. 1972, in *Case Studies in Atomic Collision Physics,* ed. E. W. McDaniel and M. R. C. McDowell (New York: American Elsevier), Ch. 4

Gilbody H. B. 1978, *Inst. Phys. Conf. Ser. No. 38,* Ch. *4,* p. 56

Henry R. J. W., Burke P. G., & Sinfailam A.-L. 1969, *Phys. Rev. A, 178, 218*

Ho Y. K., & Henry R. J. W 1983, *Astrophys. J., 264, 733*

Kriss G. A., Hartig G. F., Armus L., Blair W. P., Caganoff S., & Dressel L. 1991, *Astrophys. J., 377,* L13

Lampton M., & Bixler J. 1985, *Rev. Sci. Instr., 56, 164*

Lee A. R., Enos C.S., & Brenton A. G. 1991, *Chem. Phys., 750, 275*

Mason H. E. and Monsignori-Fossi B. C. 1994, "Spectroscopic Diagnostics in the EUV-UV for Solar and Stellar Plasmas, " private communication

McGrath M. A., Feldman P. D., Strobe] D.F., Moos H. W., & Banister G. E. 1993, *Astrophys. J., 415,* L55

McLaughlin B. M., & Bell K. L. 1993a, *J. Phys. B, 26, 1797*

McLaughlin B. M., & Bell K. L.1993b, *Astrophys. J., 408, 753.* Note that Figure 2 of this paper should read $\sigma(\AA^2)/O.$ 879735.

McLaughlin B. M., & Bell K. L. 1993c, *J. Phys. B, 26, 3313*

McLaughlin B. M., & Bell K. L. 1994a, *Mon. Not. Royal Astron. Sot., 267, 231*

McLaughlin B. M., & Bell K. L. 1994b, *Astrophs. J. Suppl. Ser., 94, S166*

McLaughlin B. M., Burke P. G., & Kingston A.E. 1987, *J. Phys. B, 20, L55*

Moos H. W., Feldman P. D., Durrance S. T., Blair W. P., Bowers C. W., Davidsen A. F., Dixon W. V., Ferguson H. C., Henry R. C., Kimble R. A., Kriss G. A., Kruk J. W., Long K. S., & Vancura O. 1991, *Astrophys. J., 382, L105*

Nilsen J. 1993, *Physics Scripts. T47, 83*

Seaton M. J. 1987, *J. Phys. B, 20, 6363*

Smith K. 1971, *The Calculation of Atomic Collision Processes (New* York and London:

Wiley), Ch. 2

Smith S. J., Chutjian A., Mawhorter R. J., Williams 1. D., & Shemansky D. E. 1993a, *J. Geophys. Res., 98, 5499*

Smith S. J., Chutjian A., Mitroy J., Tayal S. S., Henry R. J. W., Man K-F., Mawhorter R. J., & Williams 1. D. 1993b, *Phys. Rev., A 48, 292*

Smith S. J., Man K-F., Mawhorter R. J., Williams 1. D., & Chutjian A. 1991, *Phys. Rev. Letters, 67, 30*

Spangenberg K. R. 1948, *Vacuum Tubes (New* York: McGraw-Hill), Ch. 13.

Turner B. R., Rutherford J. A., & Compton D. M. J. 1968, *J. Chem. Phys., 48, 1602*

Table 1. Individual and total-quadrature experimental uncertainties.

Source of uncertainty	Uncertainty at the 1σ confidence level (%)
Counting statistics	1.0
Form factor	600
Path length	1.0
Electron-current measurement	0.5
Ion-current measurement	0.5
PSD efficiency calibration	2,0
Choice of baseline and pixel area	7.0
Angular correction R	5.0
Overlapping contribution	2.0
Metastable fraction	2.0
Dead-time correction'	-0.0
	+2.0
Total quadrature uncertainty (1 .7σ or 90% CL)	+21%
	-19%

[a]This one-sided uncertainty is added linearly to the quadrature combination of the remaining uncertainties.

Table 2. Present Experimental and Theoretical (11 CC) Cross Sections σ(E) for the $^4S^\circ \rightarrow {}^2D$" (forbidden) transition in 0//. Here and in the following tables θ_{CM}^{max} is the maximum CM angle corresponding to scattering at ϑ = 90° collection in the LAB frame; and the ratio R is defined in Eq. (6) in the text. Units of *u(E)* and 2_p Contrib. are 10^{-16} cm^2.

Energy E(eV)	θ_{CM}^{max} (deg)	R	2_p Contrib.	σ(E) Expt.	σ(E) IICC
2.9	*180.0*	1.00	0.00	0.0146	
3.3	*180.0*	1.00	0.00	0.0290	
3.7	148.4	1.11	0.00	1.27	
4.0	129.8	1.19			1.018
4.1	126.5	1.22	0.00	0.874	
4.3	121.4	1.28	0.00	0.950	
4.5	118.9	1.33			0.913
4.7"	108.1	1.53	0.00	1.10	
5.1	112.9	1.42	0.05		0.798
5.5	110.6	1.47	0.10	0.849	
5.5	110.6				0.757
5.6"	04.2	1.63	0.10	0.760	
5.7	09.8	1.49	0.07	0.781	
6.0	08.4	1.52	0.11	0.714	
6.2	08.2	1.52	0.11	0.645	
6.5	07.0	1.58	0.13	0.596	
6.8	06.4	1.60	0.04	0.726	
7.0	05.9	1.62			0.627
7.4	106.0	1.65	0.06	0.850	
9.0	102.7	1.78			0.588
10.0[b]	180.0	1.00	0.03	0.503	
12.0	100.3	2.12			0.454
15.0	98.8	2.28			0.333
17.0	98.2	2.36			0.303
20.0	97.3	2.54			0.269
25.0	96.5	2.56			0.208

[a] data taken at 4 keV ion energy. All other data taken at 8 keV energy.
[b] four-phase, with mirror for complete angular collection

Table 3. Present Experimental and Theoretical (11 CC) Cross Sections $\sigma(E)$ for the $^4S^0 \rightarrow {}^4P$ (resonance) transition in 0//. See Table 2 for legend.

Energy E(eV)	θ_{CM}^{max} (deg)	R	$^2{}_D$ Contrib.	u(E) Expt.	u(E) 11CC
13.0	180.0	1.00	0.00	0.0125	
14.7	180.0	1.00	0.00	0.149	
15.1	180.0	1.00	0.058	0.471	
15.6	128.5	*1.23*	0.058	0.651	
16.0	119.2	*1.34*			0.470
16.4	115.4	*1.35*	0.076	*0.605*	
16.5'	180.0	1.00	0.076	*0.604*	
17.0	110.1	1.37			0.497
18.0	107,3	1,39			0.512
18.3	106.6	1.36	0.061	0.531	
19.0	105.0	1.35			0.571
19.1	104.7	1.35	0.061	0.496	
20.0	103.4	1.36			0.512
20.0	103.4	1.34	0.059	0.522	
20.9_5	102.3	1.34	0.059	0.543	
21,0	102.2	1.34			0.556
21.8	101.5	1.34	0.067	0.661	
22.7	100.8	1.33	0.053	0.730	
23.0	100.6	1.34			0.561
23.7	100.2	1.33	0.053	0.502	
24.2	99.9	1.32	0.038	0.623	
25.0[b]	180.0	1.00	0.04	0.591	
25.0	99.6	1.26			0.577
25.2	99.4	1.31	0.04	0.620	
25.4	99.3	1.30	0.04	0.522	
26.1	99.1	1.30	0.04	0.665	
30.0	97.8	1.24	0.0	0.523	
30.0	97.8	1.24			0.574
35.0	96.7	1.24'	0,0	0.453	
40.0	96.0	1.24'	0.0	0.436	

[a] four-phase, with mirror for complete angular collection
[b] two-phase, with mirror for complete angular collection
[c] extrapolated from the 11 CC calculation at *30.0* eV

Table 4. Present Theoretical 11-state R-Matrix Results for the $^4S^0 \rightarrow 2P^o$ transition. See Table 2 for legend.

Energy E(eV)	θ_{CM}^{max}(deg)	R	$\sigma(E)$
5.5	138.9	1.01	0.222
7.0	111.8	1.16	0.188
9.0	105.3	1.36	0.155
12.0	101.4	1.90	0.151
15.0	99.6	2.39	0.107
20.0	97.9	3.23	0.0878
25.0	96.8	4.00	0.0704

FIGURE CAPTIONS

Figure 1

Partial energy-level diagram for *OII* showing the $^4S^0 \rightarrow 2s^2 2p^3\,^2D^o$, $^2P^o$ (forbidden) and $^4S^0 \rightarrow 2s2p^4\,^4P$ (resonance) transitions.

Figure 2

Experimental merged electron-ion beams apparatus: *L1-L5,* three-element ion focusing lenses; *DM,* 60° deflection magnet; *B,* differential pumping baffle; *D,* deflector plates; *MP,* merging trochoidal plates; *AP,* electron analyzing plates; *DP,* trochoidal plates to deflect parent electron beam out of the scattering plane and into its Faraday cup; *M/* the electron mirror; and *PSD,* position-sensitive detector.

Figure 3

Attenuation curve measured for a 4 keV *OII* beam in argon. Open circles (0) represent the case for running the ion source with high filament current and high anode voltage; the crosses (+) with a low filament current and low anode voltage. The metastable fraction *f* = 0.20 for the high-current case is indicated.

are indicated.

Figure 5

Present theoretical differential cross sections for excitation of the $^4S^o \rightarrow 2s^2 2p^3\ ^2D^o$ transition in 0// in the 11-state close-coupling approximation. Incident electron energies are indicated on each curve.

Figure 6

Present theoretical differential cross sections for excitation of the $^4S^0 \rightarrow 2s2p^4\ 4_P$ transition in 0// in the 1 1-state close-coupling approximation. Incident electron energies are indicated on each curve.

Figure 7

Experimental (.) and theoretical [, present work; -----, Henry *et al.* (1 969)1 cross sections for excitation of the $^4S^0 \rightarrow 2s^2 2p^3\ ^2D$" (forbidden) transition in 0//.

Figure 8

Experimental (0) and theoretical [, present work; -----, Ho & Henry (1 983)1 cross sections for excitation of the $^4S^0 \rightarrow 2s2p^4\ ^4P$ (resonance) transition in 0//.

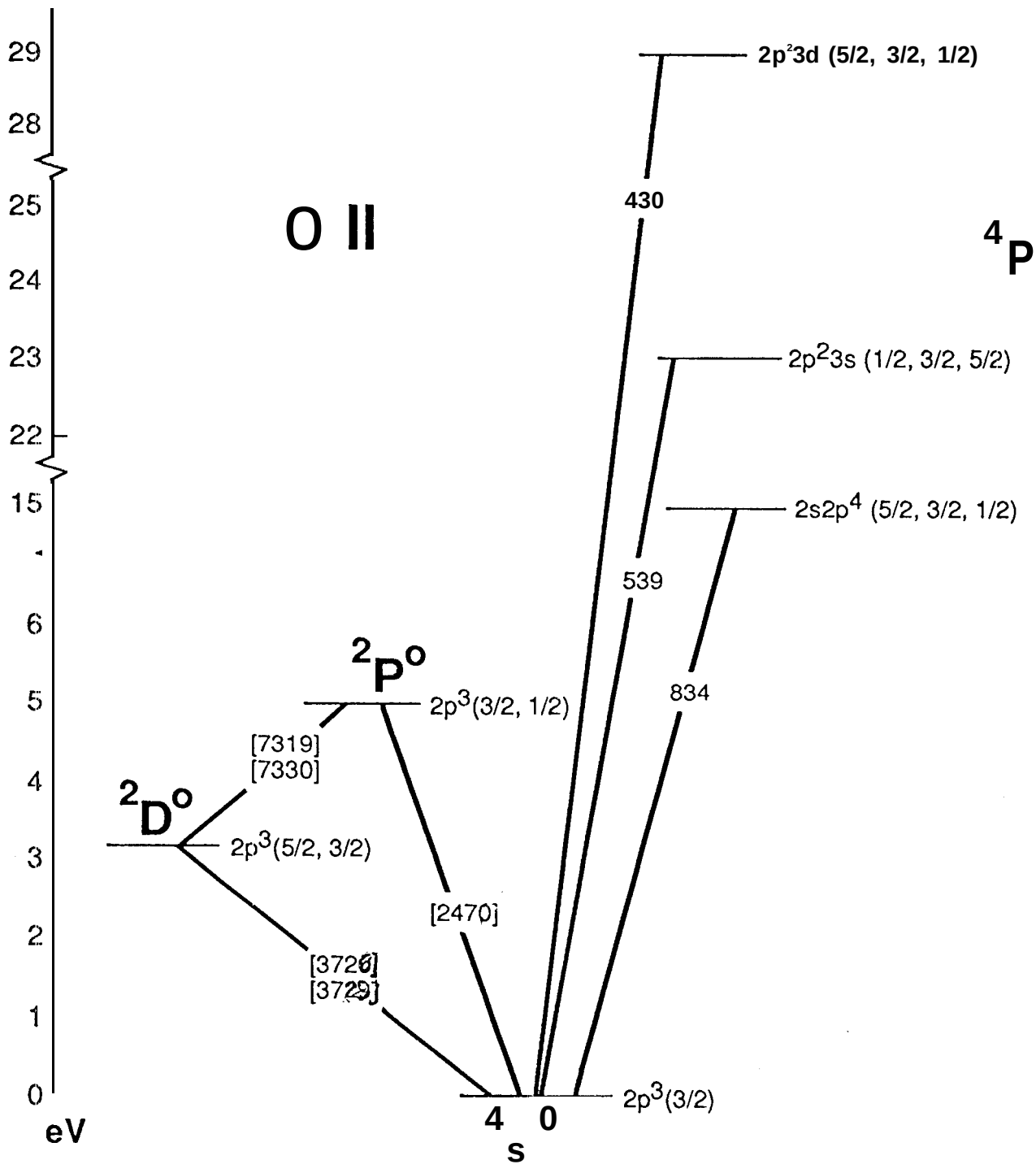
O II
29
28
25
24
23
22
15
6
5
4
3
2
1
0
eV
2p²3d (5/2, 3/2, 1/2)
430
4P
2p²3s (1/2, 3/2, 5/2)
2s2p⁴ (5/2, 3/2, 1/2)
539
834
2P°
2p³(3/2, 1/2)
[7319]
[7330]
2D°
2p³(5/2, 3/2)
[2470]
[3726]
[3729]
2p³(3/2)
4
0
s

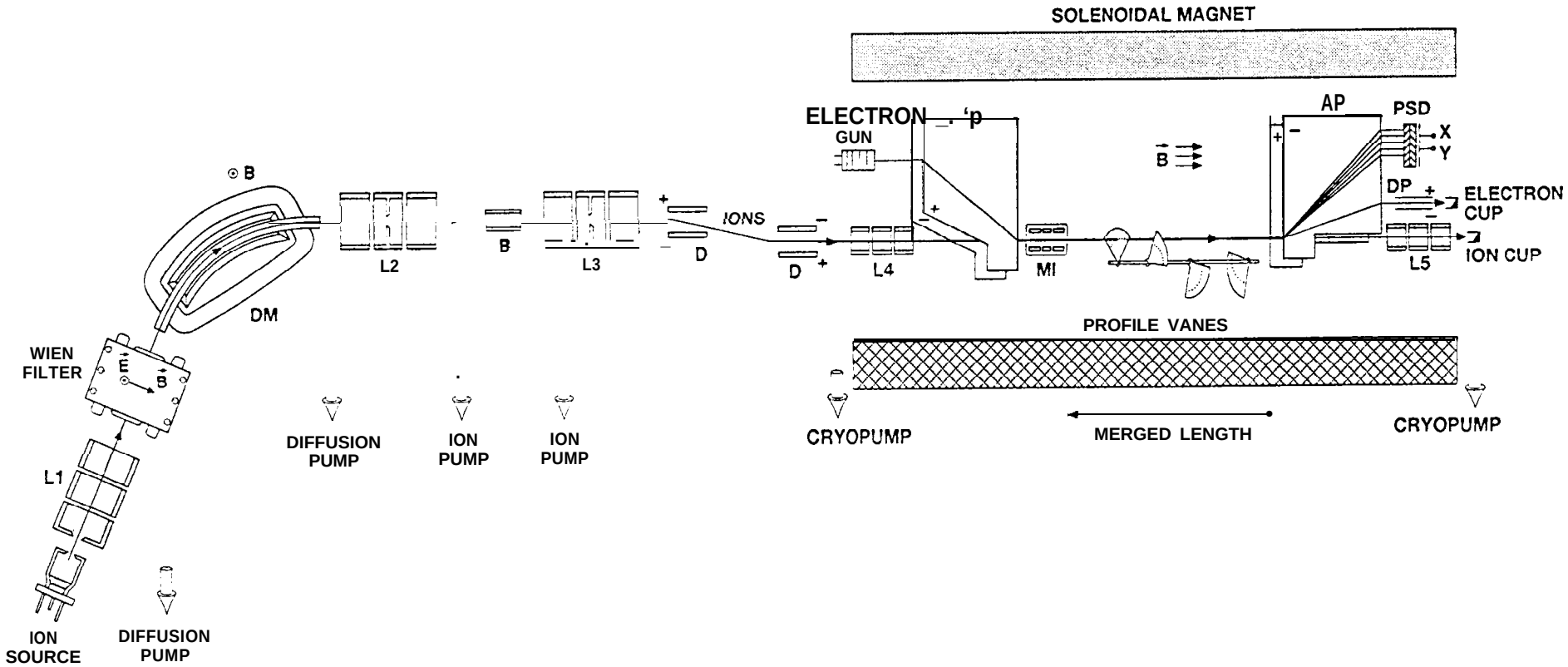
SOLENOIDAL MAGNET
ELECTRON GUN
AP
PSD
X
Y
DP
ELECTRON CUP
ION CUP
L5
B
L2
L3
D
IONS
D
L4
MI
DM
WIEN FILTER
E
B
L1
PROFILE VANES
DIFFUSION PUMP
ION PUMP
ION PUMP
CRYOPUMP
MERGED LENGTH
CRYOPUMP
ION SOURCE
DIFFUSION PUMP

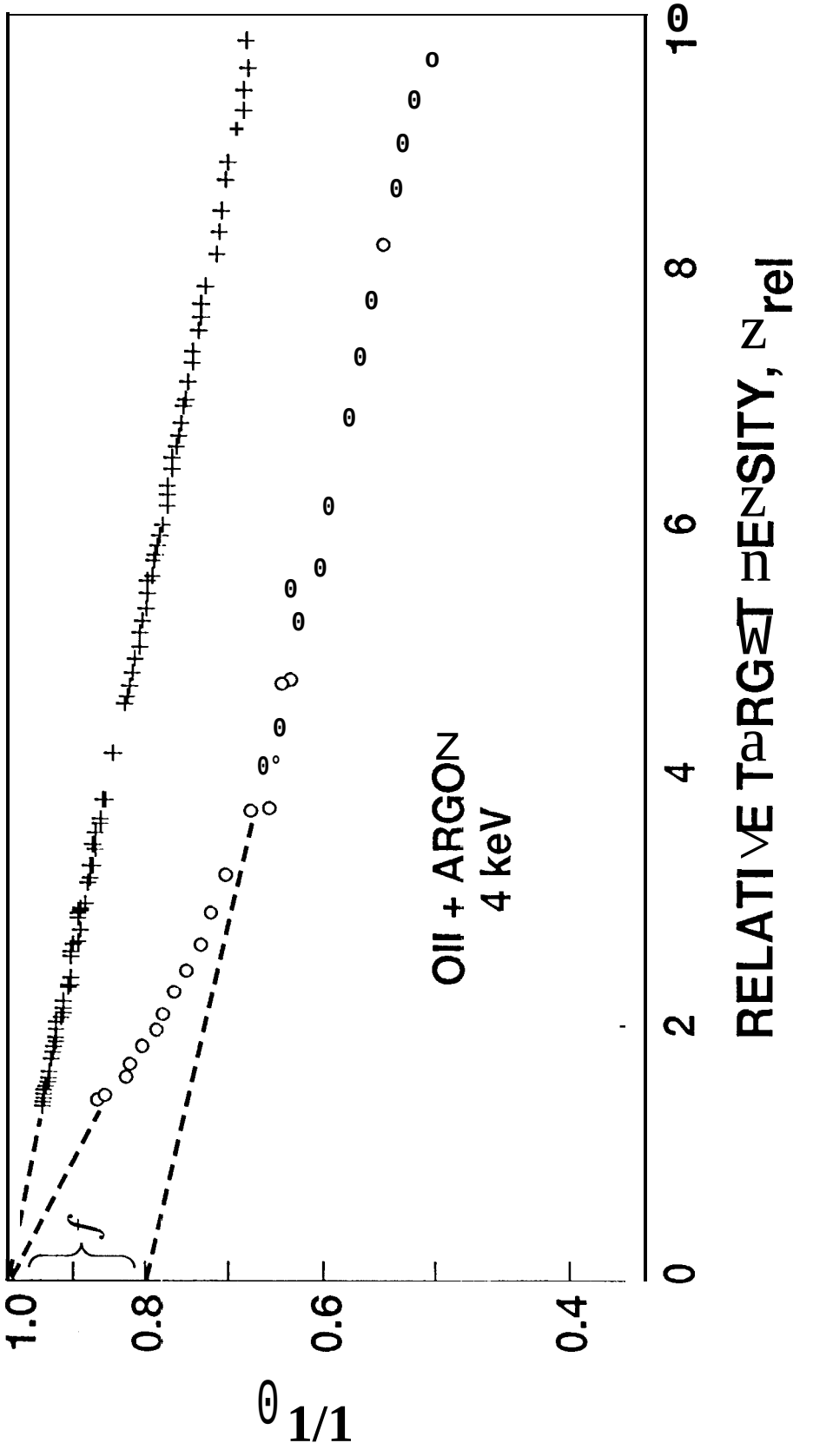
1.0
0.8
0.6
0.4
0
2
4
6
8
10
f
OII + ARGON
4 keV
RELATIVE TARGET DENSITY, n_{rel}
$\theta_{1/1}$

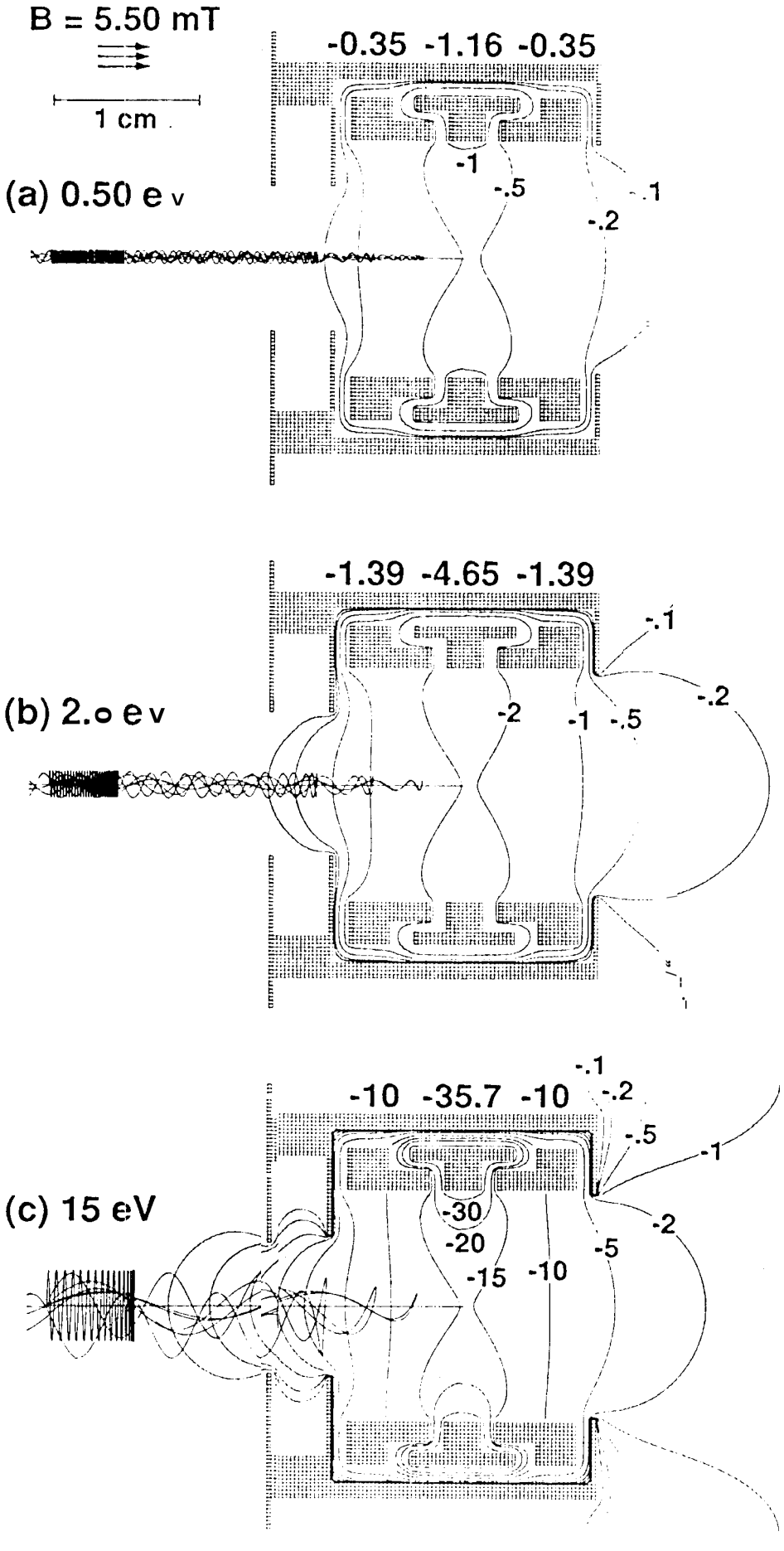
B = 5.50 mT
1 cm
(a) 0.50 e v
-0.35 -1.16 -0.35
-1
-.5
-.1
-.2
(b) 2.o e v
-1.39 -4.65 -1.39
-.1
-.2
-2
-1
-.5
(c) 15 eV
-.1
-10 -35.7 -10
-.2
-.5
-1
-30
-20
-15
-10
-5
-2

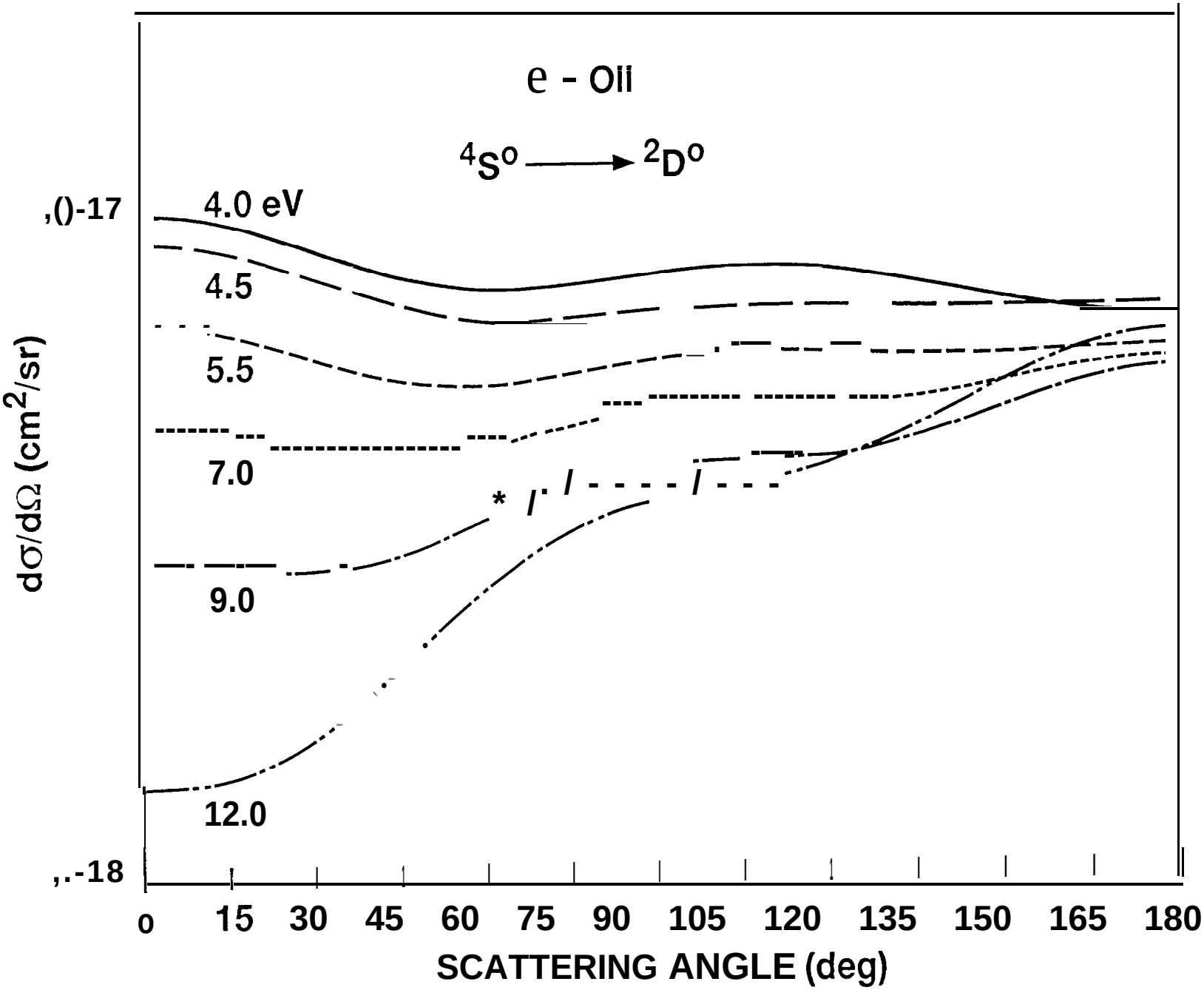
e - OII
$^4S^o \longrightarrow {}^2D^o$
4.0 eV
4.5
5.5
7.0
9.0
12.0
,()-17
,.-18
dσ/dΩ (cm²/sr)
0
15
30
45
60
75
90
105
120
135
150
165
180
SCATTERING ANGLE (deg)

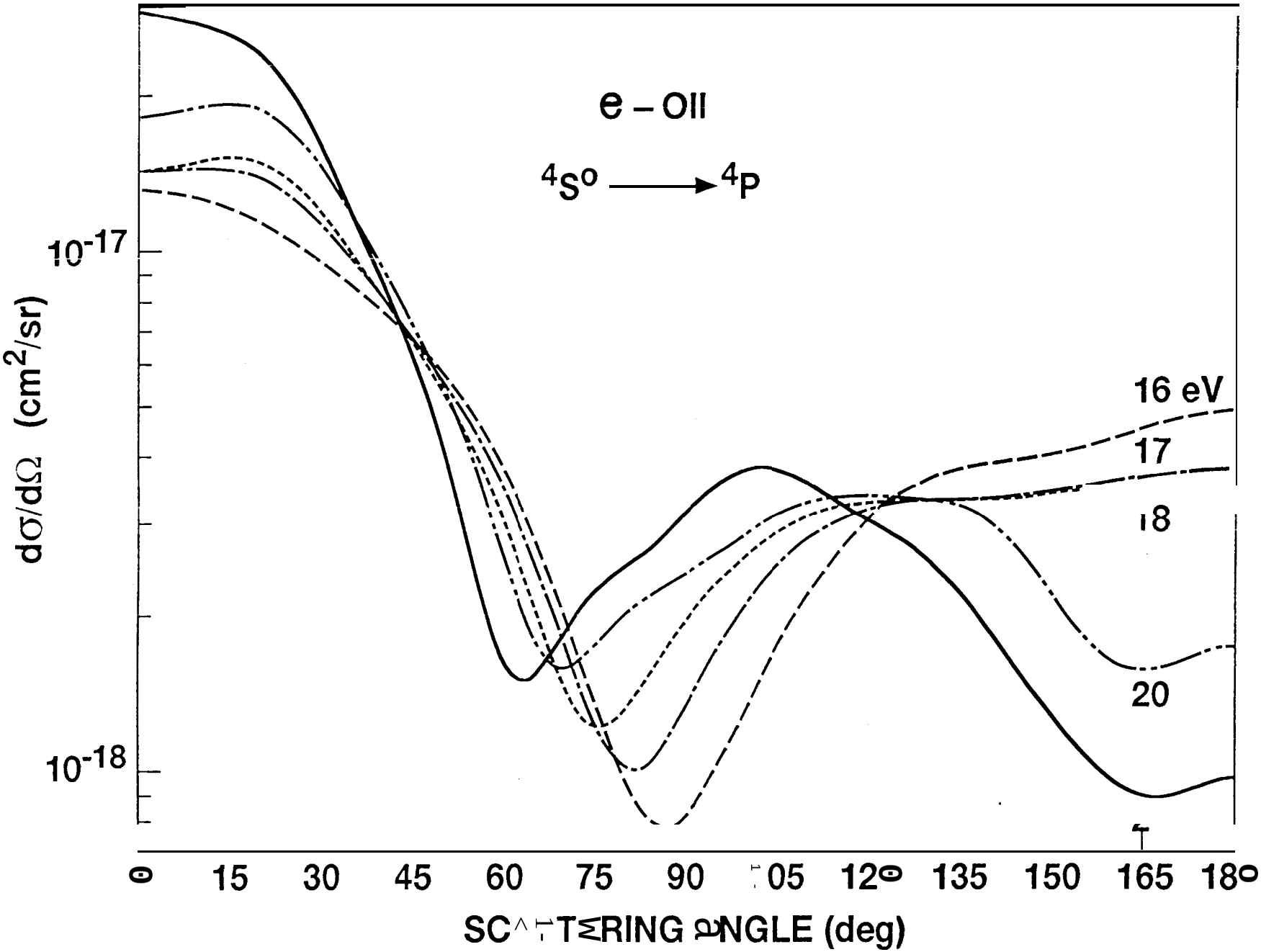
e – OII
$^4S^o \longrightarrow {}^4P$
10^{-17}
10^{-18}
$d\sigma/d\Omega$ (cm^2/sr)
16 eV
17
18
20
0
15
30
45
60
75
90
105
120
135
150
165
180
SCATTERING ANGLE (deg)

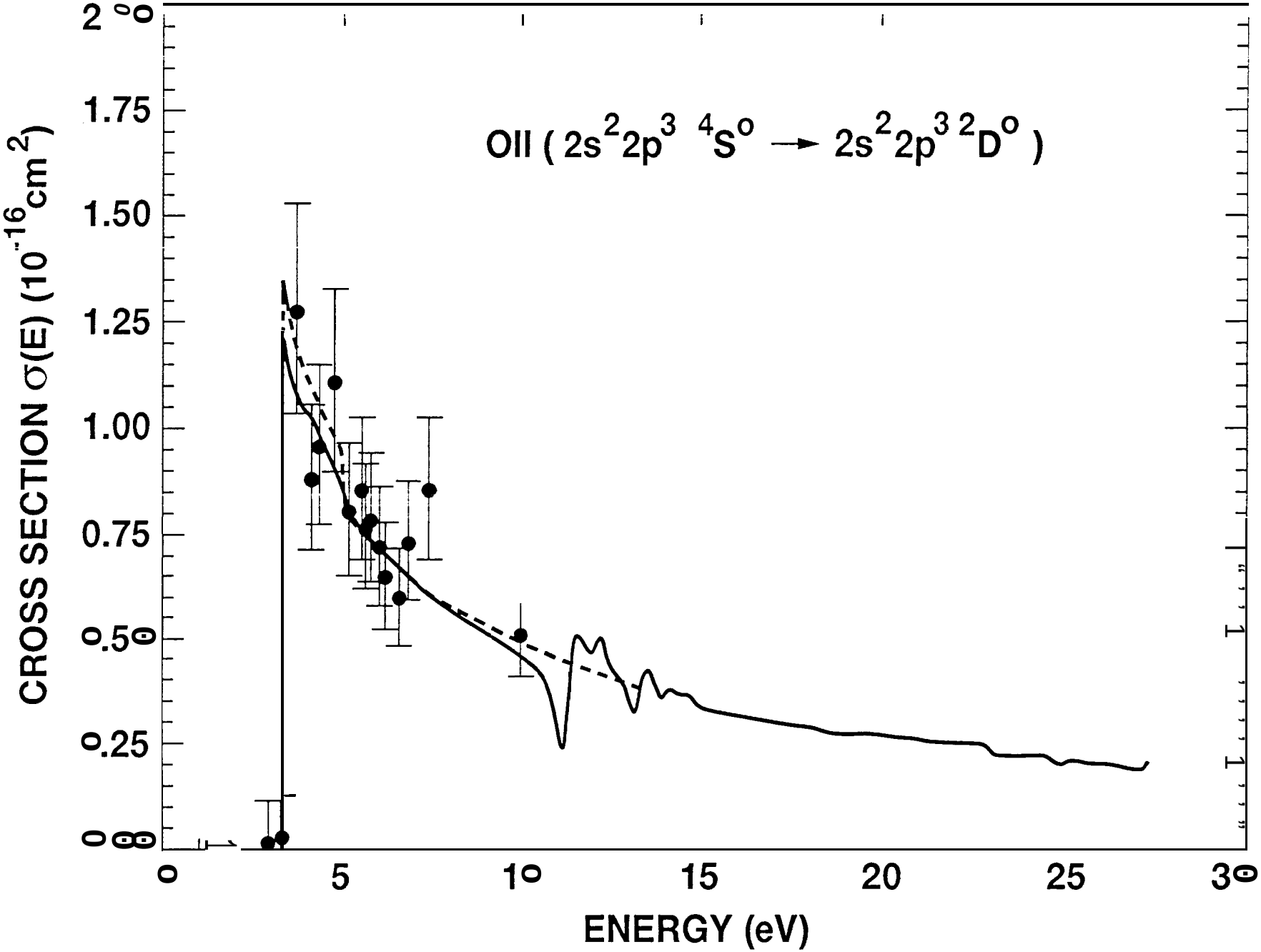
OII (2s²2p³ ⁴S° → 2s²2p³ ²D°)
CROSS SECTION σ(E) (10⁻¹⁶cm²)
ENERGY (eV)
0
0.25
0.50
0.75
1.00
1.25
1.50
1.75
2.00
0
5
10
15
20
25
30

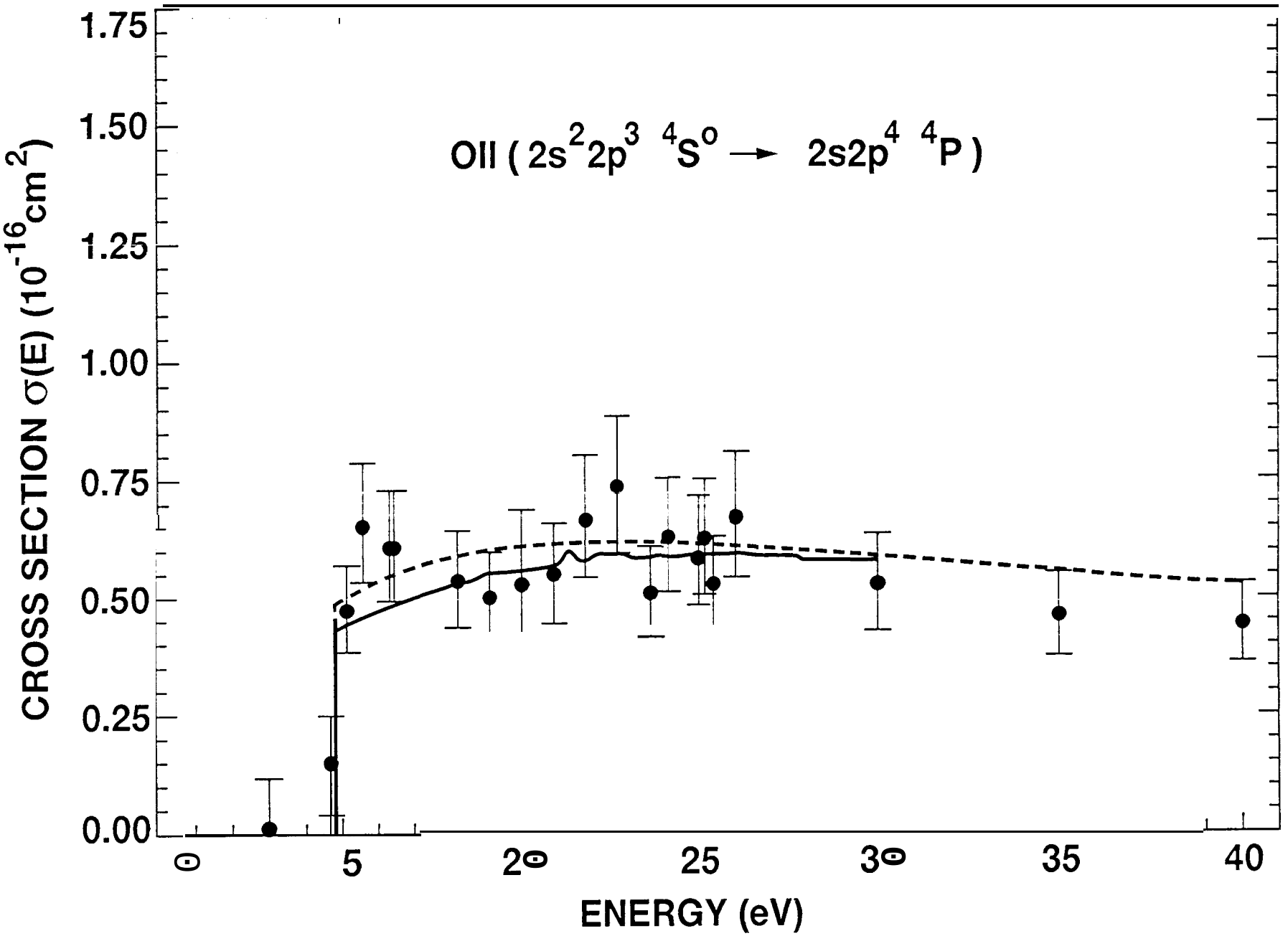
OII (2s²2p³ ⁴S° → 2s2p⁴ ⁴P)
CROSS SECTION σ(E) (10⁻¹⁶cm²)
1.75
1.50
1.25
1.00
0.75
0.50
0.25
0.00
0
5
20
25
30
35
40
ENERGY (eV)